Clim Dyn (2012) 38:2575–2591
DOI 10.1007/s00382-011-1076-3

21st Century changes in snow climate in Northern Europe: a high-resolution view from ENSEMBLES regional climate models

Jouni Räisänen · Joonas Eklund

Received: 14 February 2011 / Accepted: 11 April 2011 / Published online: 23 April 2011

Abstract Changes in snow amount in northern Europe are analysed from 11 regional model simulations of 21st century climate under the Special Report on Emissions Scenarios A1B scenario. These high-resolution models collectively indicate a future decrease in the water equivalent of the snow pack (SWE). Although winter precipitation increases, this is insufficient to compensate for the increased fraction of liquid precipitation and increased snowmelt caused by higher temperatures. The multi-model mean results suggest a slight increase in March mean SWE only locally in mountains of northern Sweden, and even there, snow is reduced earlier in winter and later in spring. The nature of the changes remains the same throughout the 21st century, but their magnitude increases with time as the greenhouse gas forcing grows larger. The geographical patterns of the change support the physically intuitive view that snow is most vulnerable to warming in areas with relatively mild winter climate. A similar relationship emerges when comparing the 11 simulations with each other: the ratio between the relative SWE decrease and winter mean temperature change is larger (smaller) for simulations with higher (lower) late 20th century winter temperatures. Despite the decrease in long-term mean SWE, individual snow-rich winters do occur in the simulations, but they become increasingly uncommon towards the end of the 21st century.

J. Räisänen (✉) · J. Eklund
Department of Physics, P.O. Box 48 (Erik Palménin aukio 1), 00014 University of Helsinki, Finland
e-mail: jouni.raisanen@helsinki.fi

J. Eklund
Finnish Meteorological Institute, P.O. Box 503 (Erik Palménin aukio 1), 00101 Helsinki, Finland

Keywords Climate change · Climate projection · Snow · Snow water equivalent · Snowfall · Regional climate model · ENSEMBLES · Northern Europe

1 Introduction

Snow is an important part of the mid- to high-latitude climate system (Vavrus 2007). The presence of snow increases surface albedo, thereby favoring lower temperatures. Snow thermally isolates the atmosphere from the ground, thus affecting cold extremes of surface air temperature even more than the winter or annual average temperature. By acting as a seasonal reservoir of water, snow also strongly modifies the hydrological cycle. Besides these physical effects, snowfall and snow impact diverse human activities. To name just two examples, abundant snowfall raises the cost of road clearance (Venäläinen and Kangas 2003), whereas scarcity of snow hampers winter outdoor tourism (Elsasser and Bürki 2002). Terrestrial ecosystems are also affected in numerous ways (Callaghan et al. 2005). For instance, many animal and plant species benefit from the thermal insulation provided by snow cover in winter, but late melting of snow also delays the beginning of the growing season in spring.

In a world with ongoing global climate change, changes are also expected in snow conditions. Some changes have already occurred (Lemke et al. 2007; Choi et al. 2010). During the past four decades, the Northern Hemisphere snow extent has decreased particularly in spring and summer, and snow has started to disappear earlier in most areas. However, there has as yet been little systematic change in the onset of snow cover in autumn or its extent in early winter. On regional scales, trends in snow conditions have been variable, probably partly due to natural climate

variability but also because of differences in the baseline climate. In mountain regions of both Europe and western North America, decreases in the length of the snow season and/or snow amount have been largest at relatively low elevations (Scherrer et al. 2004; Mote et al. 2005; Mote 2006). Higher up, where winters are colder, snow has decreased less or, in some areas, increased.

For the rest of the 21st century, climate model simulations suggest greater and more systematic changes in snow conditions, as the impact of greenhouse-gas-induced climate change is projected to grow larger. However, the changes are not expected to be geographically uniform. In analysing simulations of the water equivalent of the snow pack (SWE) by 20 global climate models (GCMs) within the Third Coupled Model Intercomparison Project (CMIP3), Räisänen (2008; hereafter R08) found a strong temperature-dependency of the 21st century changes. In areas with mild or moderate winters, the simulated SWE changes are dominated by increasing temperatures, which both increase rainfall at the expense of snowfall and enhance melting of snow. Thus, SWE is reduced throughout the winter. In the coldest regions, however, midwinter mean temperatures are projected to remain well below zero even at the end of this century, and snow conditions are therefore less sensitive to the simulated warming. For these areas, the models suggest an increase in mid-to-late winter SWE due to increasing snowfall. The average borderline between increasing and decreasing February–March mean SWE was found to coincide broadly with the −20°C isotherm in late 20th century November to March mean temperature, although with some regional variability. For early winter and late spring, the CMIP3 models suggest a decrease in SWE even in the coldest areas, due to a later shift from liquid to solid precipitation in the autumn and an earlier onset of snowmelt in spring.

Because of their coarse horizontal resolution (order of 250 km), GCMs cannot adequately describe the variation of snow conditions in areas with significant orography or complicated land-sea distribution. In the focus area of this study, northern Europe, such hetereogeneity is generated particularly by the Scandinavian mountains and the Baltic Sea. Another problem specific to northern Europe and the CMIP3 ensemble is a systematic cold bias of about 5°C in winter temperatures within this ensemble (Fig. 7 of R08). Therefore, most of the CMIP3 models probably underestimate the vulnerability of snow to warming of the north European climate.

The regional variability of climate, and potentially climate change, can be captured better by higher-resolution regional climate models (RCMs), provided that they are fed by boundary data of sufficiently high quality. During the past decade, the European Union funded PRUDENCE (Prediction of Regional scenarios and Uncertainties for Defining EuropeaN Climate change risks and Effects; Christensen and Christensen 2007) and ENSEMBLES (Ensembles-Based Predictions of Climate Changes and Their Impacts; van der Linden and Mitchell 2009) projects have produced two coordinated ensembles of RCM simulations for Europe.

Changes in snow climate in the PRUDENCE simulations were briefly analysed by Jylhä et al. (2008). Under the Special Report on Emissions Scenarios (SRES) A2 and B2 scenarios (Nakićenović and Swart 2000), the models consistently simulated both a shortening of the snow season and a decrease of snow amount in Europe between the periods 1961–1990 and 2071–2100. Most of the analysis focused on the A2 scenario and on RCM simulations driven by boundary data from the HadAM3H GCM. For this group of simulations, the average annual number of snow cover days in a Northern Europe region defined as land within (55–72°N, 0–35°E) was reduced by 45–60, depending on the RCM. The average annual SWE was reduced by 50–70%, with a larger decrease in autumn and spring than in the middle of winter. Comparable decreases in snow season length were reported for four PRUDENCE simulations made by the RCAO RCM by Räisänen et al. (2003). However, their results also revealed a large spatial variability in the change of the average annual maximum SWE. The maximum SWE was reduced relatively little (in most simulations, less than 20%) over parts of northern Scandinavia and the Scandinavian mountains, but larger decreases of the order of 60% or more were simulated in southern Sweden, Denmark, southwestern Finland and the west coast of Norway.

The ENSEMBLES RCM simulations have several advantages over the PRUDENCE data set. First, their horizontal resolution is higher (25 km vs. 50 km). Second, whereas most of the PRUDENCE simulations were based on boundary data provided by one GCM (HadAM3H), the set of driving GCMs in ENSEMBLES is larger (for this study, five). This allows a better although not comprehensive assessment of the GCM-related uncertainty. Finally, while PRUDENCE only included the two time slices 1961–1990 and 2071–2100, the ENSEMBLES simulations cover the whole 21st century. Furthermore, some aspects of the simulated climate change have been largely omitted in the PRUDENCE-based studies, including the interannual variability of snow conditions. This all warrants an analysis of changes in snow climate in the ENSEMBLES RCM simulations. In the current study, this is done for northern Europe.

After describing the data sets and some of the methodological details in Sect. 2, we analyse the snow conditions and other aspects of late 20th century winter climate in the ENSEMBLES RCMs and compare the simulations with observational data (Sect. 3). The following two sections

document the simulated time mean climate change during the 21st century, with Sect. 4 focusing on multi-model mean results and Sect. 5 on the variability between the individual simulations. In Sect. 6, the interannual variability of SWE is explored. In particular, this analysis aims to address the question how frequently individual snow-rich winters can be expected to occur in the future, despite a projected decrease in the average snow amount. A summary with discussion, including some comparison of the ENSEMBLES projections with CMIP3 and PRUDENCE, is provided in Sect. 7.

2 Data and methods

The present analysis is based on RCM simulations conducted within the ENSEMBLES project. Eleven simulations run at 25 km horisontal resolution and covering at least the years 1961–2099 were chosen, based on sufficient data availability in autumn 2009 when this research was initiated. These simulations are all based on the SRES A1B scenario. In terms of the greenhouse gas emissions and the resulting global warming, A1B is in the midrange of the SRES scenarios in the late 21st century, although it is in the upper end of the range for the next few decades (Meehl et al. 2007). The ensemble holds data from eight RCMs driven by boundary conditions from five GCMs, counting the three global and regional climate model versions from the HadCM3/HadRM3 perturbed-parameter ensemble (Collins et al. 2010) separately (Table 1). For the common analysis, all the RCM simulations were regridded to a regular 0.25° × 0.25° latitude-longitude grid, applying a bilinear interpolation scheme that only uses data from model land grid points for target grid points located on land.

In many of our figures, unweighted 11-simulation means (referred to as multi-model means) are used to characterize the typical behaviour in the simulations. A disadvantage of this choice is that the strong dependence of RCM-simulated climates on the driving GCM (Räisänen et al. 2004; Déqué et al. 2007) may make the unweighted mean unproportionally affected by those GCM simulations (specifically, ECHAM5-r3) that provided boundary conditions to several RCMs. However, tests with an alternative method of averaging (same total weight for each driving GCM) gave nearly the same results.

Where area mean seasonal cycles for the Nordic region are shown, these are calculated over the land grid boxes where (1) all 11 models have at least some snow in at least 1 month within the period 1971–2000 and (2) none of the models has permanent snow cover. This is very close to the domain shown in (e.g.) Fig. 1f, except for excluding a few grid boxes where permanent snow cover (indicative of glaciation) occurs in individual models. In the multi-model mean SWE maps, the models with glaciation are excluded in such grid boxes.

Table 1 The model simulations used in this study

Driving GCM	RCM	Institution	Shorthand
ECHAM5-r3	HIRHAM5	DMI	DMI-E5
	RACMO2	KNMI	KNMI-E5
	REMO	MPI	MPI-E5
	RCA3	SMHI	SMHI-E5
HadCM3Q3	RCA3	SMHI	SMHI-H3
	HadRM3Q3	Met Office	METO-H3
HadCM3Q0	CLM	ETHZ	ETHZ-H0
	HadRM3Q0	Met Office	METO-H0
HadCM3Q16	RCA3	C4I	C4I-H16
	HadRM3Q16	Met Office	METO-H16
BCM	RCA3	SMHI	SMHI-BCM

The first column indicates the driving global climate model, the second the regional climate model and the third the institution that conducted the simulations, using model and institution acronyms that follow the ENSEMBLES Research Theme 3 web page (http://ensemblesrt3.dmi.dk/). HadCM3Q3, HadCM3Q0 and HadCM3Q16 are three members of the HadCM3 perturbed-parameter ensemble (Collins et al. 2010) with low, intermediate and high sensitivity to increasing greenhouse gas concentrations, respectively. HadRM3Q3, HadRM3Q0 and HadRM3Q16 are the corresponding versions of the HadRM3 RCM. The last column gives the shorthand notations used in this article

In Sect. 3, model-simulated late 20th century (1971–2000) temperature and precipitation are compared with the University of East Anglia Climate Research Unit climatology (version CRU TS2.1, Mitchell and Jones 2005). These data were interpolated from their slightly coarser 0.5° × 0.5° latitude-longitude grid to the 0.25° × 0.25° grid. In addition, the simulated SWE in Finland is compared with gridded SWE data compiled by the Finnish Environment Institute, SYKE. These data are based on interpolation of operational snow course measurements in space and time, taking into account observations of temperature and precipitation and local topographic effects, as detailed by Reuna (1994). These analyses are available for the years 1991–2005, at 10 km horizontal resolution. For comparison with the model results, they were aggregated to the 0.25° × 0.25° grid boxes.

In the end of this study, the ENSEMBLES SWE projections are briefly compared with corresponding multi-model mean projections from PRUDENCE and CMIP3. The CMIP3 multi-model mean represents the average SWE change from 19 GCMs, including all the models used in R08 except for one with permanent snow cover in northern Scandinavia. The baseline period used in calculating the change (1971–2000) and the emission scenario (A1B) are

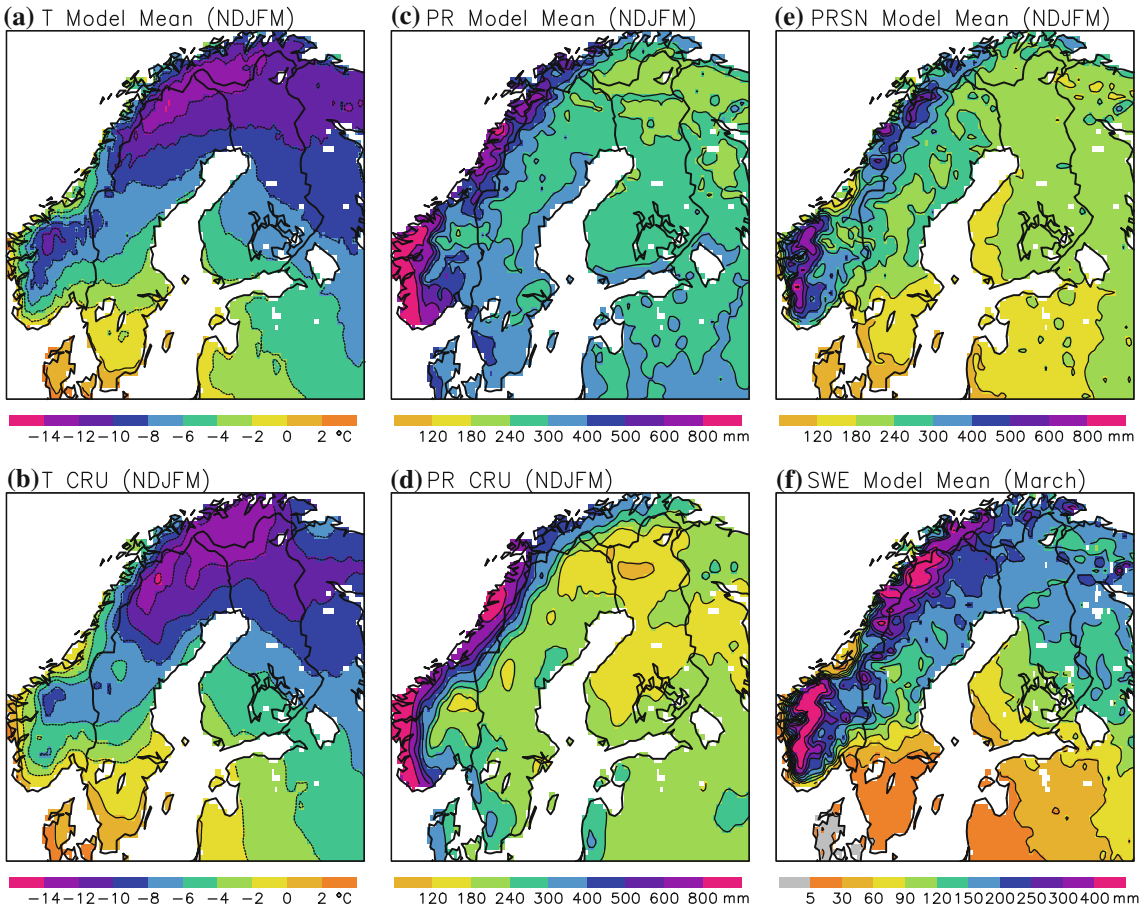

Fig. 1 Time mean winter climate in northern Europe in the years 1971–2000. Panels **a**, **c**, **e**, and **f** show 11-model means of November-March mean temperature (**a**), precipitation (**c**) and snowfall (**e**), and March mean snow water equivalent (**f**). CRU TS2.1 analyses of November–March mean temperature and precipitation are shown in **b** and **d**, respectively. Units are indicated in the *colour bars*

the same as those for ENSEMBLES. For PRUDENCE, the mean of SWE change from eight RCM simulations based on the SRES A2 scenario is calculated. Six of these simulations use boundary data from the HadAM3H GCM, two boundary data from ECHAM4/OPYC3 (see Table 1 of Jylhä et al. 2008 for details). The baseline period for the PRUDENCE experiments is 1961–1990. Bilinear interpolation was used to regrid the CMIP3 and PRUDENCE data to the 0.25° grid.

3 Winter climate in the late 20th century

Following R08, we use mean values over the November–March (NDJFM) season to provide an overview of winter climate, except for SWE for which values for March are used to capture its seasonal maximum in most of our domain. In Fig. 1, multi-model NDJFM means of temperature, total precipitation and snowfall during the period 1971–2000 are given. For the first two, observational estimates from CRU TS 2.1 are also shown. In most of the Nordic area, the simulated temperatures are close to or slightly below the observational estimate. However, the cold bias is much smaller than that found for the CMIP3 GCM simulations by R08. The observed geographical pattern of temperature, with the coldest conditions in the northern inland and the Scandinavian mountains, is very well simulated.

For precipitation, the agreement is worse. Excluding the coast of western Norway, the simulated precipitation generally exceeds the observational estimate, the Nordic mean difference being 31%. However, at least part of this difference reflects the severe undercatch of solid precipitation in rain gauge measurements (Adam and Lettenmaier 2003). This observational bias is not known precisely, but may be comparable to the apparent model-observation difference seen in Figs. 1c, d. For example, Ungersböck et al. (2001) found that gauge measurements of precipitation in the Baltic Sea drainage basin during the NDJFM season should be corrected upward by 20–50%.

The simulated NDJFM snowfall (Fig. 1e) reflects the variations in both temperature and precipitation, being

largest over the Norwegian mountains but relatively small in Denmark and southern Sweden. The SWE in March shows partly the same geographical pattern, but with a stronger contrast between cold and mild areas (Fig. 1f). In regions with colder climate, a larger fraction of the accumulated snowfall stays on ground in late winter.

The multi-model March mean SWE in Finland is compared with the SYKE analysis in Fig. 2. The agreement is excellent, both for the geographical pattern and the absolute values, although some of the local topographically induced maxima are missed at the 25 km resolution of the models. This good agreement suggests that winter precipitation in the models is more realistic than implied by Fig. 1c, d. Of course, the risk of compensating errors (e.g., too much simulated precipitation balanced by too efficient snowmelt) must be borne in mind.

As illustrated by area mean seasonal cycles in Fig. 3, the late 20th century climate varies substantially between the individual simulations. Some of these differences clearly originate from the driving GCM. For example, all four simulations with boundary data from ECHAM5-r3 are among the five warmest throughout the autumn and winter (Fig. 3a). However, the RCM also matters. In particular, precipitation is much larger in DMI-E5 than in any other simulation, but the three other ECHAM5-r3-driven simulations are near the multi-model mean (Fig. 3b). Even more remarkably, both the smallest (MPI-E5) and largest (DMI-E5) Nordic mean SWEs occur in simulations driven by ECHAM5-r3 (Fig. 3d), with a factor of two and half difference between these two. However, the seasonal cycle of both the Nordic and Finland mean SWE (Fig. 3e) is similar in shape in nearly all the simulations, with a gradual rise to a peak in March and a more rapid decrease thereafter. An exception is ETHZ-H0, which clearly exhibits delayed snowmelt in comparison with the other simulations and (at least for Finland) observations. Unsurprisingly, this delayed snowmelt coincides with a large cold bias in spring (Fig. 3a). However, the root cause of this behaviour would need separate investigation.

For SWE in Finland, the SYKE analysis falls in the middle of the wide range of simulated values (Fig. 3e). For Nordic mean temperature as well, the observational estimate is within the range of the model simulations, although near its upper end in spring (Fig. 3a). By contrast, the Nordic mean precipitation in all 11 simulations exceeds the CRU TS 2.1 estimate. Biases in observations may largely explain this systematic difference in winter. However, this is unlikely to be the case in spring, when the relative difference between the 11-model mean and CRU TS 2.1 increases despite a decrease in the fraction of solid precipitation that is expected to reduce measurement errors (Ungersböck et al. 2001).

4 Climate change in the 21st century: a multi-model mean view

A multi-model mean view of the changes in winter climate during the 21st century is given in Figs. 4 and 5. Shown in the first three rows of Fig. 4 are the changes in NDJFM

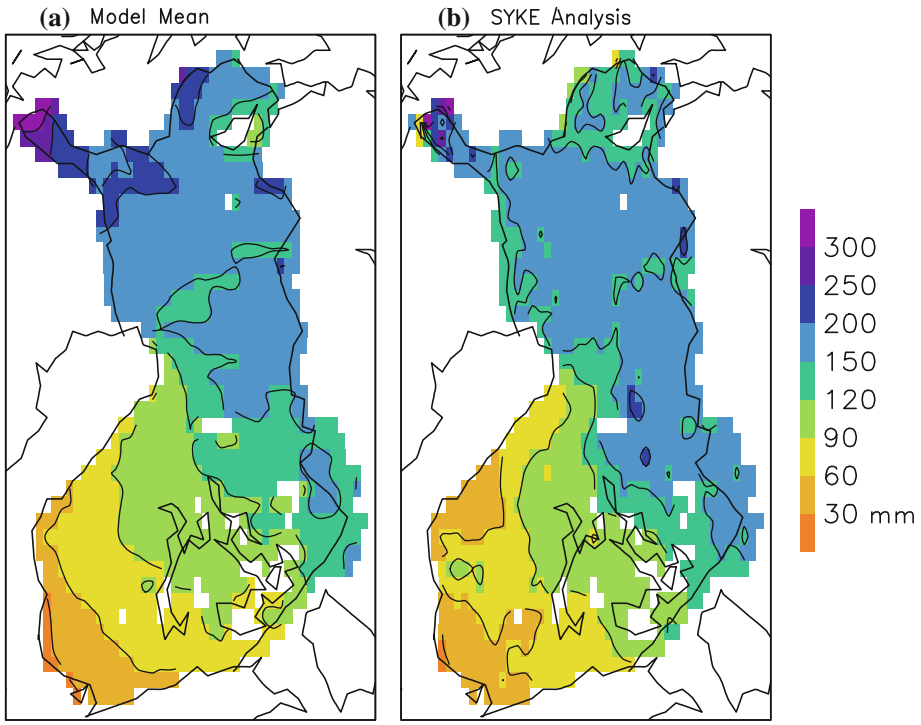

Fig. 2 March mean snow water equivalent (mm) in Finland in the years 1991–2005. **a** 11-model mean, **b** SYKE analysis

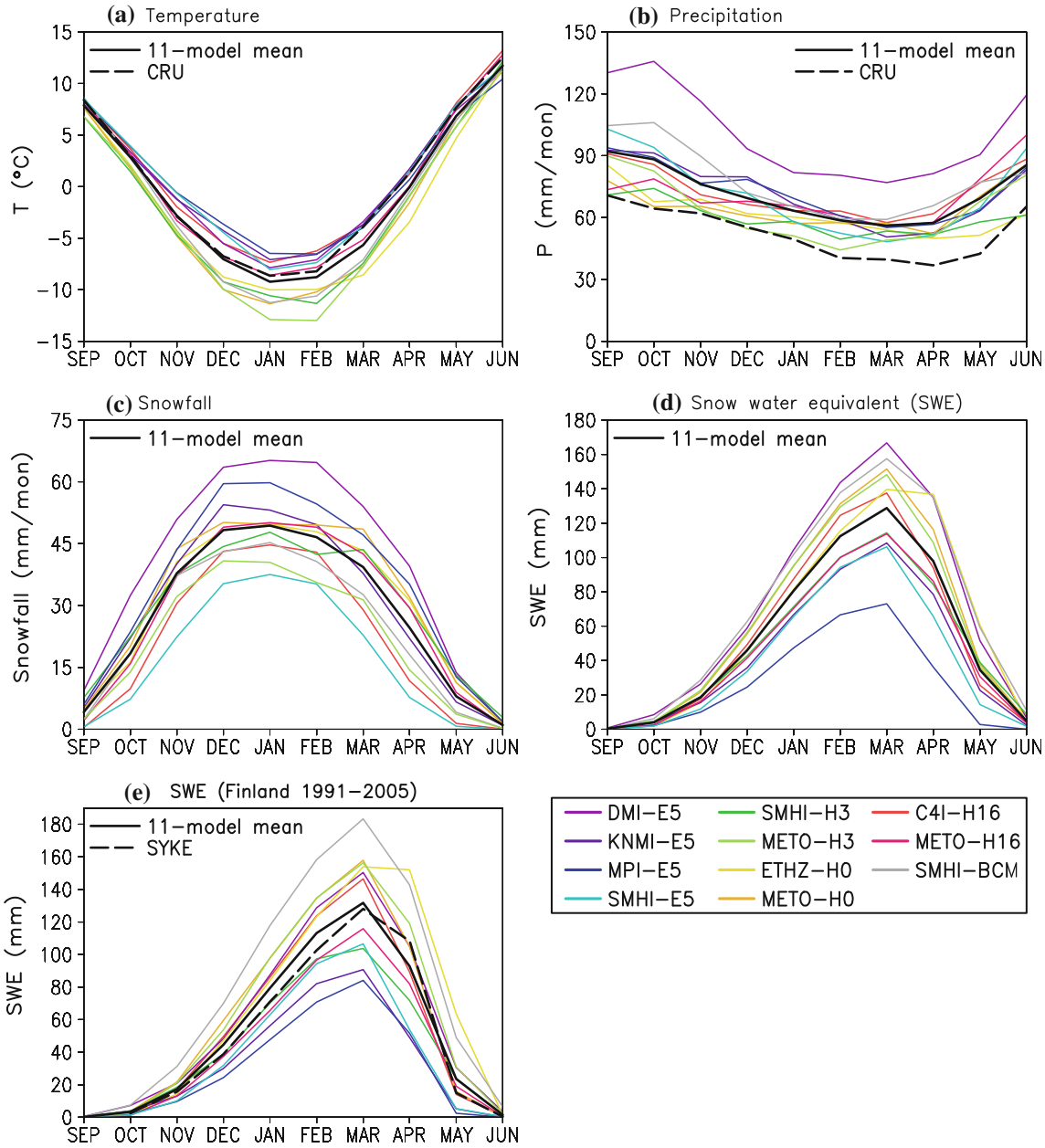

Fig. 3 Area mean seasonal cycles of **a** temperature, **b** precipitation, **c** snowfall and **d** snow water equivalent in the Nordic area in 1971–2000, and of **e** snow water equivalent in Finland in 1991–2005. The *coloured lines* represent the 11 RCM simulations as indicated by the legend, and the *black solid lines* the 11-model means. Observational estimates are shown by dashed lines in **a**, **b** and **e**

temperature, precipitation and snowfall from 1971 to 2000 to three later 30-year periods: 2010–2039, 2040–2069 and 2070–2099. The corresponding changes in March mean SWE are illustrated in the last row.

For all four variables, the sign and geographical pattern of the multi-model mean change remain largely the same throughout the 21st century, but the changes increase in magnitude with time. The NDJFM mean temperature is simulated to increase by about 1–2°C by 2010–2039, by 2–4°C by 2040–2069, and by 3–6°C by 2070–2099, with the smallest warming in the southwest and the largest in the northeast of the domain.

A slight increase in total precipitation is already simulated in 2010–2039, and the change grows larger with time. In 2070–2099, it exceeds 20% in most of the Nordic area, but a marked northwest-southeast gradient occurs accross the Scandinavian mountains. Whereas precipitation locally increases by 40% in northern Sweden, the increase along the northwestern coast of Norway is generally less than 10%. Earlier RCM simulations have shown that

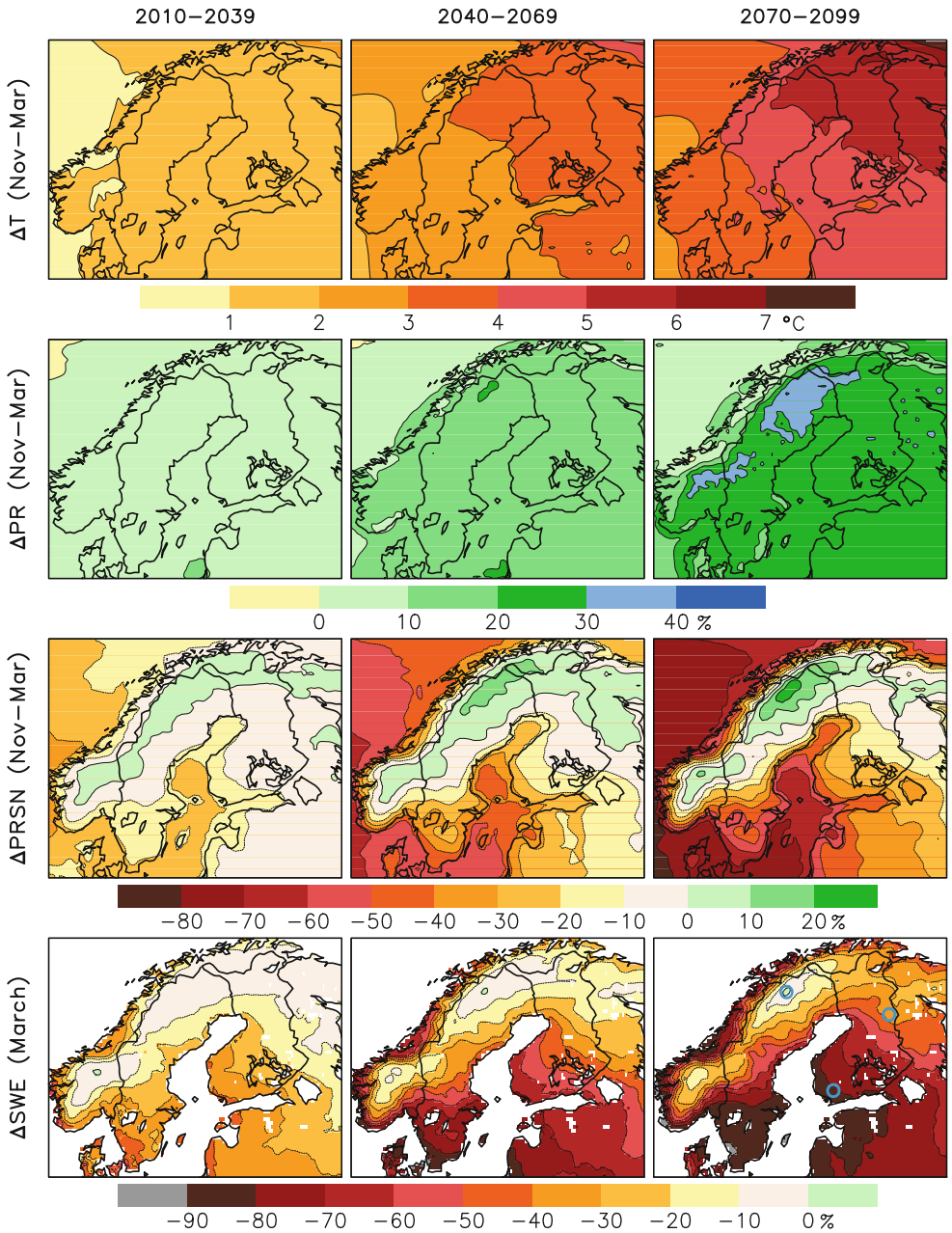

Fig. 4 11-model mean changes in (rows 1–3) November–March mean temperature, precipitation and snowfall, and (row 4) March mean snow water equivalent. The changes represent differences from the mean values in the years 1971–2000 and are shown for the periods 2010–2039 (*left*), 2040–2069 (*middle*) and 2070–2099 (*right*). The units are given in the *colour bars*. The *blue open circles* in the *bottom-right panel* indicate the locations of the three *grid boxes* used in Figs. 5 and 6

precipitation change in this area is highly sensitive to changes in the atmospheric circulation (Räisänen et al. 2004). Yet, the northwest-southeast gradient in the ENSEMBLES simulations may not be easily explained by time mean circulation changes alone. The multi-model NDJFM mean sea level pressure change by 2070–2099 is small, 0 to −1 hPa, in all of the Nordic area, and suggests little change in the time mean flow across the Scandinavian mountains (not shown). A closer study of the origin of this precipitation change gradient would therefore be warranted.

Despite the increase in total precipitation, NDJFM snowfall is reduced in most of the Nordic area. In the years 2070–2099, the multi-model mean decrease exceeds 50% in Denmark and southern Sweden, and along the coastlines of the Baltic states and Norway. Further north and further inland, where the present-day climate is colder, the phase of precipitation is less sensitive to warming and the

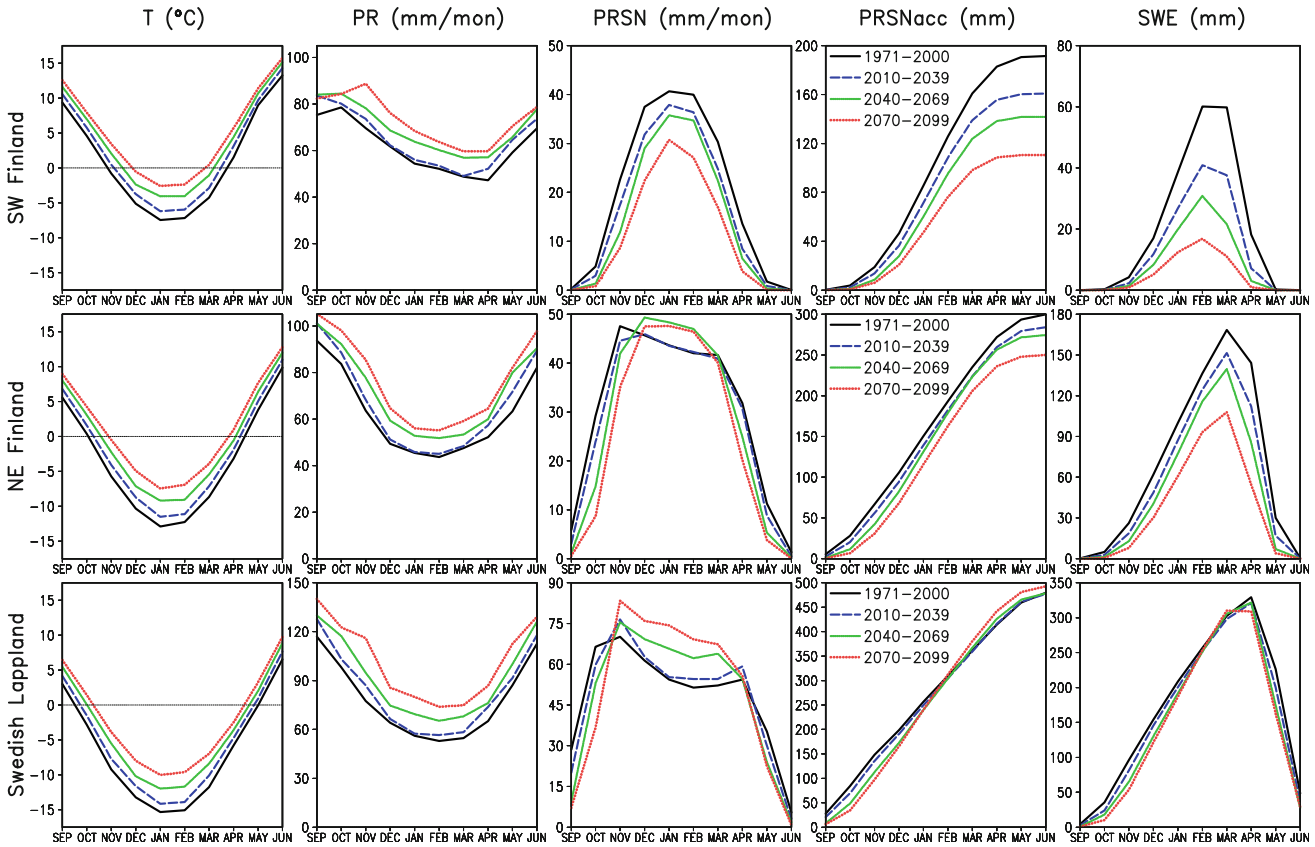

Fig. 5 11-model means of temperature (*T*), precipitation (*PR*), snowfall (*PRSN*), accumulated snowfall (*PRSNacc*) and snow water equivalent (*SWE*) averaged over the periods 1971–2000 (*black*), 2010–2039 (*blue*), 2040–2069 (*green*) and 2070–2099 (*red*). From *top* to *bottom*: SW Finland at (60.9°N, 23.4°E), NE Finland at (65.9°N, 29.1°E), and Swedish Lappland at (67.4°N, 18.6°E). The time axis runs from September to June

decrease in snowfall is smaller. In some inland areas north of the Arctic Circle and over the Scandinavian mountains snowfall is simulated to increase, although less than total precipitation. The largest increase, exceeding 20% in 2070–2099, occurs in northwestern Sweden.

As early as in 2010–2039, March mean SWE is reduced in virtually all of the Nordic area. The change is still less than 10% in northern inland areas and over the Scandinavian mountains, but it locally reaches 40% further south. Towards the end of the twentyfirst century, much larger decreases in snow amount are simulated. Southwestern Finland, southern Sweden, western parts of the Baltic states and coastal Norway lose 80% or more of their March mean SWE by 2070–2099, and the decrease also exceeds 50% in wide areas in central Finland and Sweden. The change over the Scandinavian mountains and in the northernmost inland areas is more modest. A marginal increase in the multi-model average March mean SWE occurs locally in northwestern Sweden, in the area with the largest simulated increase in snowfall.

The seasonal cycle of the multi-model mean changes is depicted in Fig. 5, for three grid boxes that are marked with blue circles in the bottom-right panel of Fig. 4. The first, named "SW Finland", is located in the municipality of Jokioinen in southwestern Finland (60.9°N, 23.4°E), and is characterized by relatively mild present-day winters and a severe simulated decrease in SWE during the 21st century. The second ("NE Finland") is in the municipality of Kuusamo (65.9°N, 29.1°E), with considerably colder and snowier present-day winters and a less dramatic simulated decrease in SWE. The third location ("Swedish Lappland") is on the eastern slopes of the Scandinavian mountains, at (67.4°N, 18.6°E). Here, the multi-model mean suggests a small increase in March mean SWE during the 21st century.

Common to all three locations and all the variables studied in Fig. 5 is a gradual increase in the magnitude of the changes from the early to the late 21st century, with slight irregularity due to residual effects of natural variability in the 30-year multi-model means. Also common is a maximum of temperature increase in winter and slightly smaller warming in autumn and spring. Precipitation is also simulated to increase throughout the September–June period portrayed in the figure. The relative change is largest in

Swedish Lappland, where even the baseline precipitation is larger than in the other two locations.

In terms of the snowfall change (columns 3–4 of Fig. 5), the three locations differ. In SW Finland, snowfall is reduced throughout the winter, although in January the decrease from 1971–2000 to 2070–2099 is only 25%. Here, a much larger part of the total precipitation falls as rain in a warmer climate. In the other two locations, with colder winters, the decrease in the fraction of solid precipitation is smaller. Thus, the increase in total precipitation also translates into an increase in snowfall, in NE Finland from December to February and in Swedish Lappland from November to April. Earlier in the autumn and later in the spring, however, snowfall is reduced substantially at both locations.

To complement the monthly sums of snowfall, the snowfall accumulated from the beginning of the autumn is shown in the 4th column of Fig. 5. Following R08, these values represent the snowfall summed from August to the month on the time axis, but with half-weight for the last month to approximate mid-month values. In both SW and NE Finland, the accumulated snowfall is reduced regardless of the month considered—the increase in midwinter snowfall in NE Finland is outweighed by the decrease in autumn. In Swedish Lappland as well, accumulated snowfall in the three 21st century periods remains below the 1971–2000 mean until January, but it slightly exceeds the baseline values later in winter and spring, especially in 2070–2099.

Finally, the average seasonal cycle of SWE in the three locations is shown in the last column on Fig. 5. In the two Finnish grid boxes, SWE is reduced in relative terms more than the accumulated snowfall. In SW Finland, for example, the maximum value of SWE (which shifts from March in 1971–2000 to February in the 21st century) is reduced by almost 75% in 2070–2099, although the snowfall accumulated by February is only reduced by 40%. Thus, more frequent and more intense melting periods in the simulated milder winters reduce the fraction of snow that survives on the ground. The increase in snowmelt also affects SWE in Swedish Lappland, but here its impact only becomes substantial in spring. Because of the earlier onset of intense springtime snowmelt, SWE decreases beginning from April, although more snow has fallen during the winter.

Following the formulation detailed in Eqs. (1)-(2) of R08, the change in SWE between two periods of time (ΔSWE) can be decomposed into four terms:

$$\Delta SWE = \Delta SWE(\Delta P) + \Delta SWE(\Delta F) + \Delta SWE(\Delta G) + \Delta SWE(NL). \quad (1)$$

Here the first three right-hand-side terms represent the contributions from the changes in total precipitation (ΔP), fraction of solid precipitation (ΔF), and the fraction of accumulated snowfall that remains on the ground (ΔG). $\Delta SWE(NL)$ involves a non-linear combination of ΔG, ΔF and ΔP, but is typically much smaller than the first three terms.

In Fig. 6, (1) is used to decompose the multi-model mean SWE change from 1971–2000 to 2070–2099 at the three locations studied in Fig. 5. $\Delta SWE(\Delta P)$ is positive in all cases: all else being the same, the increase in total precipitation would have led to an increase in SWE. In the two Finnish grid boxes, however, this term is overwhelmed by negative contributions from $\Delta SWE(\Delta F)$ and $\Delta SWE(\Delta G)$. The former, representing the increase in rainfall at the expense of snowfall, dominates in the early winter until January. The latter, reflecting the effect of more efficient snowmelt, grows larger towards the end of the winter, becoming the main cause of reduced SWE in

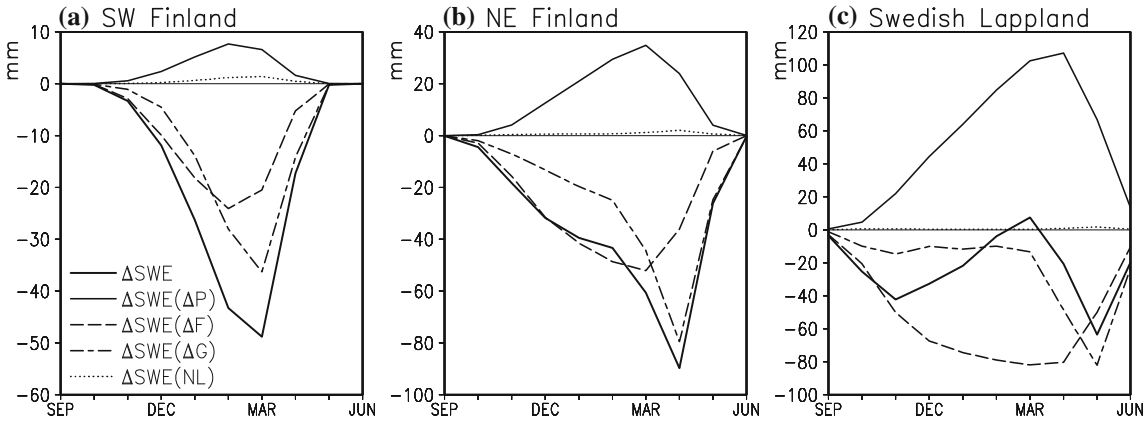

Fig. 6 11-model mean changes in snow water equivalent (in mm) decomposed with Eq. (1) to the contributions of precipitation change (ΔP), change in the fraction of solid precipitation (ΔF), change in the fraction of accumulated snowfall that remains on the ground (ΔG), and the nonlinear term (*NL*). **a** SW Finland at (60.9°N, 23.4°E), **b** NE Finland at (65.9°N, 29.1°E), and **c** Swedish Lappland at (67.4°N, 18.6°E)

spring. Both $\Delta SWE(\Delta F)$ and $\Delta SWE(\Delta G)$ also act to reduce SWE in the grid box in Swedish Lappland, although $\Delta SWE(\Delta G)$ remains small until March. Together, they dominate over $\Delta SWE(\Delta P)$ for most of the winter, thus explaining the decrease in SWE. In March, however, $\Delta SWE(\Delta P)$ is large enough to compensate for the negative contributions of the other terms. Thus, SWE increases, although this small change represents a delicate balance between competing factors.

A similar decomposition for the periods 2010–2039 and 2040–2069 gives qualitatively the same results, although all terms in (1) are smaller in magnitude (not shown).

5 Climate change in the 21st century: variation between individual model simulations

The projected climate change varies between the 11 RCM simulations. For a first illustration, the range of March mean SWE changes is shown in Fig. 7. Note that the minimum (i.e., most negative) and maximum changes are selected separately for each grid box. Thus, the maps as whole do not represent any single simulation.

For any single grid box and any of the three periods, the range of the simulated changes covers several tens of per cent of the baseline SWE. In much of the Nordic area, the range grows wider with time, as the increase in greenhouse gas forcing makes the climate response increasingly sensitive to model differences. Over parts of the Scandinavian mountains, this means an amplification of both the largest simulated increase and decrease with time. For example, in the "Swedish Lappland" grid box studied in Figs. 5 and 6, the 11-simulation range of March mean SWE change in 2070–2099 extends approximately from −30 to 30%.

Despite the variation in the magnitude of the change, a decrease in SWE is robust in large parts of the Nordic area (top row of Fig. 8). As early as in 2010–2039, there are wide areas where March mean SWE decreases in all 11 simulations, and these areas further expand in the later 30-year periods. In the late 21st century, increases in SWE in the individual simulations are almost entirely restricted to the eastern slopes of the Scandinavian mountains. At this time, only a couple of grid boxes remain in northern Sweden where SWE increases in a majority (6 out of 11) of the models.

Even where a large majority of models agree on the sign of the change, this does not guarantee that the change is large enough to be clearly discernible from natural variability (cf. Brown and Mote 2009). To explore this issue, a standard t test was applied to each model simulation separately, using 5% significance threshold in a two-sided test and neglecting interannual autocorrelation. Then, the number of models with significant changes was counted (rows 2–3 of Fig. 8). In 2010–2039, there are only limited areas with a statistically significant decrease in March mean SWE in a majority of the models, mostly in western Norway and south-central Finland. Later, significant decreases in SWE become more common. In 2070–2099, all 11 simulations agree on a significant decrease in SWE in about a half of northern Europe. By contrast, significant increases in SWE are very rare. They only occur in more than one model simultaneously in northwestern Sweden.

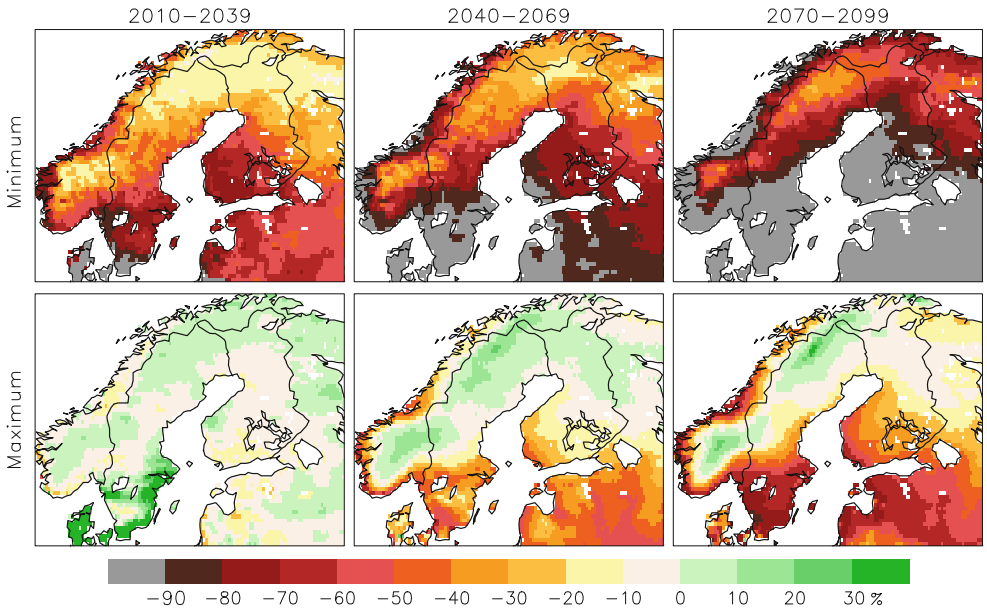

Fig. 7 Range of March mean SWE change among the 11 models. The *first row* shows, for each *grid box* separately, the minimum (i.e., the most negative) and the *second row* the maximum (or least negative) change in the individual models

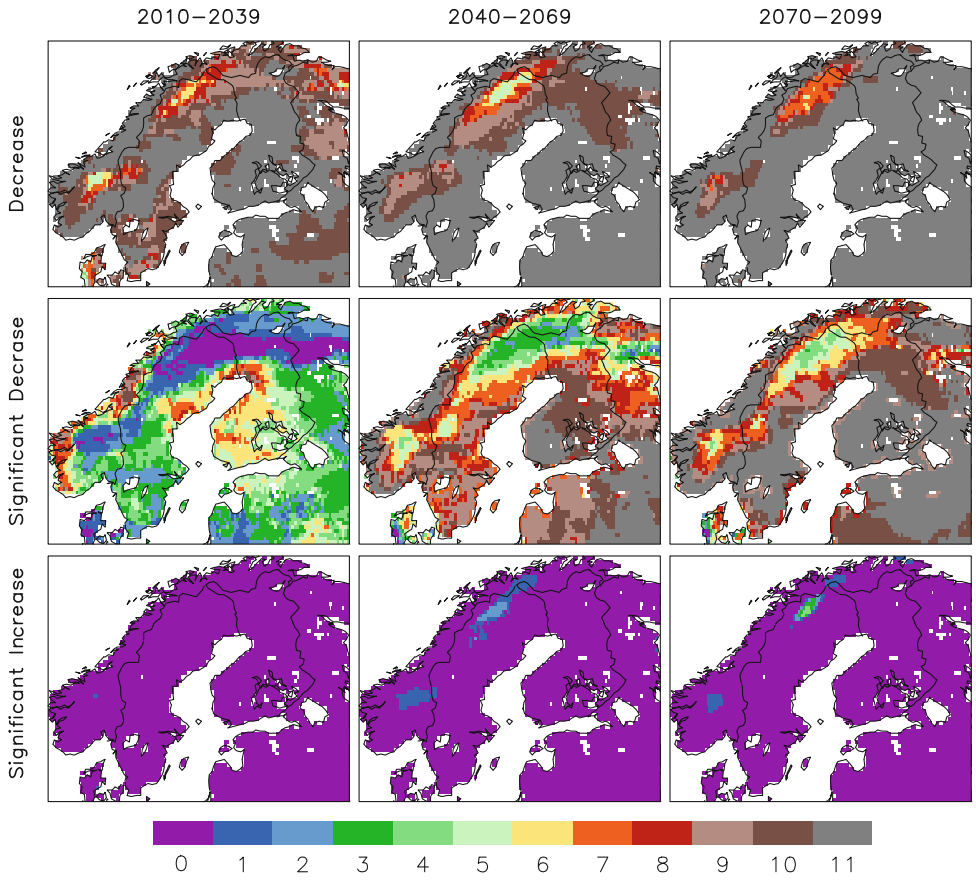

Fig. 8 Number of models (out of 11) in which (*top*) SWE decreases by any amount (*middle*) SWE decreases significantly and (*bottom*) SWE increases significantly

There, locally up to 4 of the 11 models simulate a significant increase in March mean SWE in 2070–2099, although significant decreases are also found in several models.

In Fig. 9, seasonal cycles of the Nordic mean climate change from 1971–2000 to 2070–2099 are shown separately for all 11 simulations. For temperature, in particular, the dependence of the RCM-simulated change on the driving GCM is overwhelming, as seen in Fig. 9a from a tendency for lines with similar colour to cluster together. The warming is strongest in METO-H16, and the C4I-H16 simulation with the same boundary data is also near the upper end of the range. Conversely, the four simulations using ECHAM5-r3 boundary conditions (lines with bluish colours) exhibit less warming than most of the others. Still, the range of temperature change among the 11 simulations is relatively narrow, particularly in winter when the difference between the models with the smallest and largest warming is less than a factor of two. For comparison, the "likely" range of 21st century global mean warming as assessed by Meehl et al. (2007) was 1.1–6.4°C when considering all six SRES scenarios, and 1.7–4.4°C for the A1B scenario alone. Thus, the variation between the ENSEMBLES simulations clearly understates the actual uncertainty in future temperature change, in particular as the uncertainty is expected to increase towards smaller scales (Räisänen 2001).

The Nordic mean precipitation change varies more among the 11 simulations than the temperature change, although some increase in precipitation occurs in all simulations throughout the September-June period (Fig. 9b). Concurring with Déqué et al. (2007), the influence of the driving GCM is less dominant than for temperature change. For example, both the smallest and the largest increase in January precipitation are found in simulations with ECHAM5-r3 boundaries. A curious peak in the multi-model mean change occurs in November, reflecting mainly the behaviour of the ECHAM5-r3- and HadCM3Q16-driven simulations. Given the large variability of the seasonal cycles of precipitation change between the individual models, little confidence can be given to such monthly details.

Both the Nordic mean snowfall and SWE exhibit the largest per cent decrease in autumn and late spring, and a smaller decrease in winter (Fig. 9c, d). As already seen from Figs. 4 and 5, SWE is reduced systematically more than snowfall. However, the changes in these two variables are correlated among the RCM simulations, with the largest decreases in SWE in METO-H16 and C4I-H16 that also simulate a large reduction in snowfall.

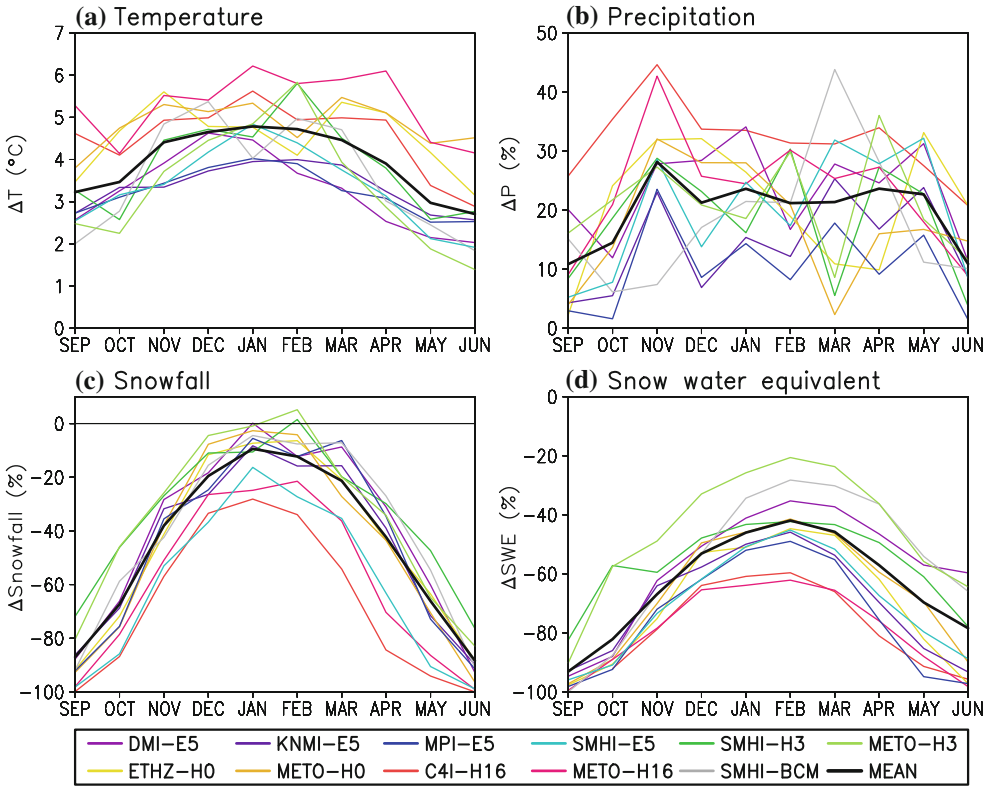

Fig. 9 Changes in northern Europe mean **a** temperature (°C), **b** precipitation (%), **c** snowfall (%) and **d** snow water equivalent (%) from 1971–2000 to 2070–2099 in the 11 models separately

Generally, one would expect the decrease in SWE to amplify with increasing warming. However, Fig. 10a only confirms this to the extent that the METO-H16 and C4I-H16 simulations with the largest decrease in Nordic March mean SWE are both among the three simulations with the greatest NDJFM warming. An important reason for this lack of correlation are differences in baseline climates between the 11 simulations. As shown in Fig. 10b, the March mean SWE change is more strongly correlated with the baseline NDJFM temperature than the temperature change. An even stronger negative correlation ($r = -0.86$) is found when comparing the baseline NDJFM temperature with the ratio between the SWE change and the simulated warming (Fig. 10c). Thus, the SWE is most (least) sensitive to the warming in the models with the highest (lowest) baseline temperatures. This is analogous to the geographical distribution of the simulated SWE change, with larger (smaller) decreases in SWE in areas with milder (colder) present-day winters (cf. Figs. 1 and 4; see also R08).

The Nordic mean NDJFM temperature in 1971–2000 as calculated from the CRU TS 2.1 analysis was −6.1°C, or just 0.6°C above the multi-model mean. However, the warmest and the coldest simulations have temperatures much further from the observations. Fig. 10c suggests that the wide range in the SWE change to temperature change ratio might be partly an artifact of this large range in baseline temperatures, rather than representing a genuine uncertainty. On the other hand, as discussed above, the range in the simulated warming (from 3.7 to 5.8°C for the Nordic mean NDJFM mean values) clearly underestimates the actual uncertainty in future temperature change.

6 Interannual variability of snow conditions

This far, our focus has been on 30-year means of SWE and other variables. However, weather conditions in northern Europe vary greatly from one winter to another, mainly due to the variation of atmospheric circulation (Hurrell 1995; Seager et al. 2010). An example is given in Fig. 11, which shows time series of maximum SWE in the "NE Finland" grid box for all 11 simulations and the whole period 1971–2099. The maximum SWE is defined here as the highest monthly mean SWE for each winter, which may occur in different months depending on weather conditions. Being based on monthly data, this diagnostics naturally underestimates the maxima of SWE on the daily time scale.

Fig. 11 reveals a huge variation of absolute SWE values between the individual simulations. In MPI-E5, the average maximum value in 1971–2000 (as shown by the horizontal

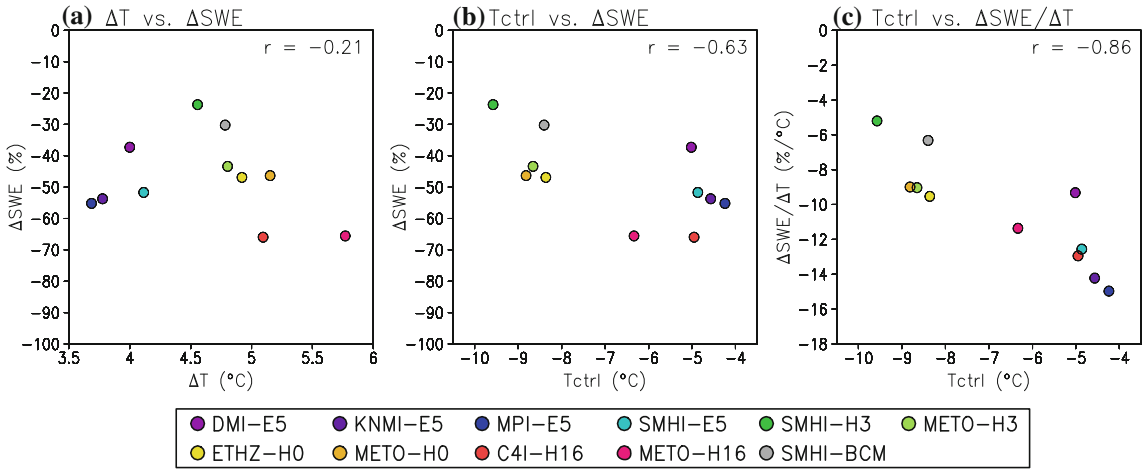

Fig. 10 **a** Relationship between the NDJFM Nordic mean temperature change (*horizontal axis*) and March mean SWE change from 1971–2000 to 2070–2099 among the 11 models. The correlation between the two quantities is given in the *upper right corner*. **b** as **a**, but between the 1971–2000 NDJFM mean temperature and the SWE change. **c** as **b**, but between between the 1971–2000 NDJFM mean temperature and the March mean SWE change normalized by the NDJFM mean temperature change

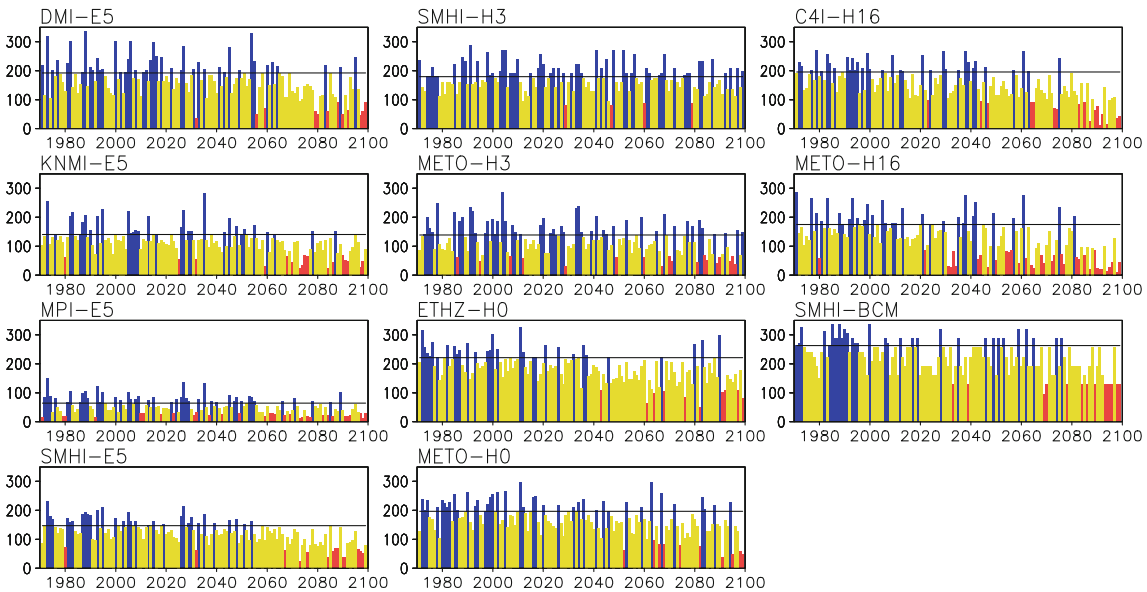

Fig. 11 Interannual variability of maximum monthly mean SWE (unit: mm) in NE Finland (65.9°N, 29.1°E) in the 11 simulations. The average for the period 1971–2000 is indicated by *horizontal lines*. Winters with a SWE maximum greater than this are marked with *blue bars*, those with a SWE maximum of less than 50% of the period 1971–2000 mean with *red bars*, and all other winters with *yellow bars*

line) is only 70 mm, in SMHI-BCM as much as 260 mm. Because this makes it difficult to interpret the simulated 21st century SWE maxima in absolute terms, a relative classification is applied instead. For each simulation separately, winters with maximum SWE larger than the 1971–2000 mean are defined as "snow-rich" and are shown by blue bars. Similarly, "very snow-poor" winters with maximum SWE less than half of the 1971–2000 mean are shown by red bars, whereas the remaining winters are coded with yellow colour.

As expected, the simulations collectively indicate a gradual decrease in the frequency of snow-rich winters and an increase in the frequency of very snow-poor winters, although with substantial variation between the individual models. A geographically wider perspective on the multi-model mean change is given in Fig. 12, showing the average numbers of snow-rich and very snow-poor winters for four 30-year periods separately. Because the yearly SWE maxima are bounded from below by zero, their distribution tends to be positively skewed. Therefore, slightly

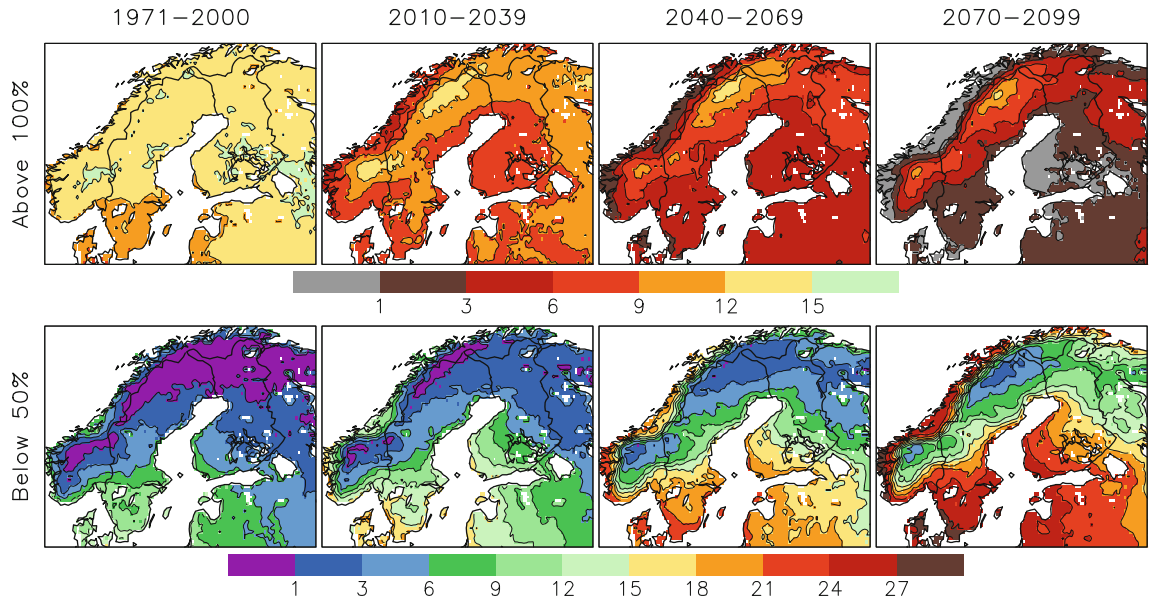

Fig. 12 11-model mean number (cases per 30 years) of winters with maximum monthly mean SWE greater than the corresponding mean for 1971–2000 (*top*), and less than half of the mean for 1971–2000 (*bottom*). Note the difference in colour scale between the *two rows*

less than half of the simulated winters in 1971–2000 are classified as snow-rich in most areas, but the difference is only substantial in the mildest parts of the Nordic domain.

As time progresses, snow-rich winters become gradually less frequent, following a geographical distribution that broadly mimics the change in mean SWE in Fig. 4 (Fig. 12, top). In 2070–2099, their average simulated number only exceeds 3 per 30 years in a relatively limited area over the Scandinavian mountains and northern inland regions. Notably, such winters virtually disappear by that time in all of western Norway. On the other hand, a substantial number of snow-rich winters is simulated in northernmost Sweden even in 2070–2099. In interpreting these results, recall that snow-rich is defined relative to the mean value in 1971–2000, so that a snow-rich winter in (e.g.) southern Sweden might have much less snow than a snow-poor one in northern Sweden.

The number of winters with a SWE maximum of less than half of the 1971–2000 mean is highly variable in this period itself (Fig. 12, bottom), reflecting the different variability of snow climate in different parts of the area. Far in the north and over the Scandinavian mountains such winters are very rare, but up to about 12 of them occur per 30 years in southernmost Sweden and Denmark. A similar pattern is seen in the later 30-year periods, but the absolute number increases everywhere. In 2070–2099, more than 80% of all simulated winters are classified into this category in Denmark, southern Sweden, southwestern Finland, and western parts of Norway and the Baltic states. In the mountains of northern Swedish Lappland, however, such winters are still infrequent, occurring less than thrice in 30 years.

As already noted, the changes in the frequency of snow-rich and very snow-poor winters vary between the individual simulations. Returning to the "NE Finland" grid box in Fig. 11, in SMHI-E5 the last winter with a SWE maximum above the mean of 1971–2000 is simulated in the year 2054, whereas 18 such winters occur after this year in SMHI-H3. A more systematic analysis of this variation is provided in Table 2, also including the other two grid boxes studied in Figs. 5 and 6. A steep and robust increase in the number of very snow-poor winters accompanies a decrease in the number of snow-rich winters in SW Finland, whereas smaller changes to the same direction take place in NE Finland. However, the variation between the individual simulations is large enough to preclude more than an order-of-magnitude prediction of these changes. In the Swedish Lappland grid box, even the sign of the changes is ambiguous.

7 Summary and discussion

The evolution of snow amount, as measured by the snow water equivalent (SWE), has been analysed for 11 RCM simulations of 21st century climate in northern Europe. The simulations indicate an increase in winter precipitation in the area, but this is counteracted by a pronounced warming of the winters. As a result of the warming, a larger fraction of the precipitation falls as rain and episodes of snowmelt

Table 2 Number (cases per 30 years) of winters with maximum monthly mean SWE above 100% or below 50% of the corresponding mean for 1971–2000

	SW Finland (60.9°N, 23.4°E)		NE Finland (65.9°N, 29.1°E)		Swedish Lappland (67.4°N, 18.6°E)	
	>100%	<50%	>100%	<50%	>100%	<50%
1971–2000	14.5 (11–16)	6.0 (0–11)	14.1 (10–17)	0.8 (0–4)	14.7 (12–18)	0.2 (0–1)
2010–2039	7.5 (1–15)	12.7 (3–23)	9.5 (5–13)	2.0 (0–7)	13.6 (6–20)	1.0 (0–4)
2040–2069	3.8 (1–9)	18.5 (8–25)	7.1 (2–13)	4.0 (4–13)	14.5 (8–25)	1.8 (0–7)
2070–2099	1.0 (0–3)	24.8 (11–28)	3.8 (0–11)	9.8 (1–17)	13.5 (4–23)	1.2 (0–4)

In each table cell, the first value is the 11-model mean number, and the range between the models is given in parentheses

become more common. Thus, the amount of snow is generally reduced, with the magnitude of the decrease growing with time following the projected increase in greenhouse gas forcing. However, there is substantial regional variability in this change within northern Europe. The mildest areas, including Denmark, southern Sweden, southwestern Finland, western parts of the Baltic states and coastal Norway, are projected to lose almost all of their snow by the late twentyfirst century. At the other extreme, about a half of the 11 simulations indicate an increase in SWE in March in northern Swedish Lappland.

Where do our projections stand in relation to earlier model simulations? Fig. 13 compares the ENSEMBLES multi-model average March mean SWE change in 2070–2099 with corresponding multi-model means from the PRUDENCE and CMIP3 data sets, as detailed in Sect. 2. In the PRUDENCE simulations, SWE tends to decrease slightly more than in ENSEMBLES. However, this is at least partly explained by the higher emission scenario (A2 rather than A1B) and earlier baseline period (1961–1990 rather than 1971–2000) used in the PRUDENCE experiments. The local increase in SWE in northern Sweden is absent from the PRUDENCE multi-model mean. This might be partly due to the coarser resolution of the PRUDENCE models (50 vs. 25 km), although it is important to note that the small increase in the ENSEMBLES multi-model mean represents a delicate balance between increases and decreases in the individual simulations. As a whole, however, these two RCM ensembles agree quite well, suggesting that the difference in their resolution is relatively unimportant for the magnitude and general patterns of SWE change within northern Europe.

The agreement between the two RCM ensembles and CMIP3 is worse, but this is not unexpected. The smaller decrease in SWE in CMIP3 is most likely associated with the cold bias in this ensemble (Fig. 7 of R08). The eastward shift in the area of smallest SWE decrease in the CMIP3 simulations, from northern Sweden to Finland and Russia, is also not surprising given the poor representation of the Scandinavian mountains at the coarse GCM resolution.

Based on this comparison and the good simulation of present-day winter climate, we judge the ENSEMBLES multi-model mean to give a credible "best-guess" view of how snow conditions in northern Europe might change in the future. Nevertheless, the uncertainty around this best guess should not be disregarded. The changes vary between the 11 RCM simulations, although part of this variation is attributable to differences in the baseline temperature climate. More importantly, the 11 simulations are very unlikely to cover the full range of uncertainty in future climate change in northern Europe. The simulations are all based on the same (SRES A1B) emissions scenario, and the RCMs were driven by only five different GCMs. The Nordic mean NDJFM warming to the end of the 21st century varies by only a factor of 1.6 (3.7–5.8°C) among the 11 simulations (Fig. 10a). This is narrower than the "likely" range of 21st century global mean warming under the A1B scenario as assessed by Meehl et al. (2007), 1.7–4.4°C, despite the expected increase in uncertainty towards smaller horizontal scales. The contrast to the range of 1.1–6.4°C that covers all six SRES scenarios is even more striking.

The impacts of snow on nature and society are not determined by climatological mean SWE alone, but are also affected by the interannul variability of snow conditions. Individual snow-rich winters (defined here as winters with the maximum monthly SWE above the local mean in 1971–2000) are still simulated to occur in the coming decades even where there is a decrease in the long-term mean SWE. In large parts of the Nordic region, however, such snow-rich winters are projected to become quite uncommon by the end of the 21st century.

Another point of practical importance is the distinction between snow amount and snowfall. Snowfall is projected to decrease less or (in the coldest areas) increase more than SWE. In most of the Nordic region, substantial amounts of snow are still likely to fall even in the late 21st century, even where increased melting precludes the formation of a deep long-lasting snow cover. Furthermore, although this issue has not been addressed here, changes in the total

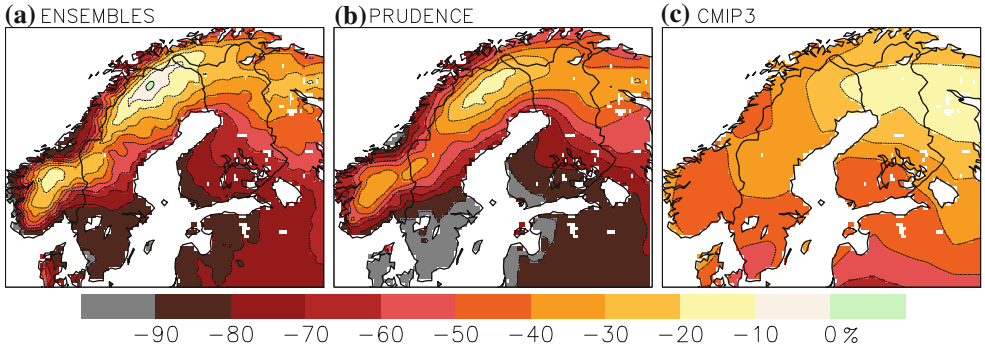

Fig. 13 Ensemble mean change in March mean SWE in **a** the ENSEMBLES and **b** the PRUDENCE RCM simulations, and **c** in the CMIP3 GCMs. The changes for ENSEMBLES and CMIP are from 1971–2000 to 2070–2099 under the A1B scenario, those for PRUDENCE from 1961–1990 to 2071–2100 under the A2 scenario

amount of snowfall do not directly tell what happens to heavy short-term snowfall. For example, the results of Makkonen et al. (2007) suggest an increase in extreme 6-h snowfall in large parts of the Nordic area, despite a general decrease in total annual snowfall.

Acknowledgments The RCM simulations used in this study were obtained from the European Union funded ENSEMBLES (Contract number 505539) and PRUDENCE (EVK2-CT2001-00132) project data archives. The World Climate Research Programme CMIP3 data set is supported by the Office of Science, U.S. Department of Energy. Noora Veijalainen, Hannu Sirviö and Heidi Sjöblom at the Finnish Enviroment Institute helped us with the SYKE snow data. The work of JE was funded by the ACCLIM2 project within the Finnish Climate Change Adaptation Research Programme ISTO and by the Nordic Climate and Energy Systems (CES) project.

References

Adam JC, Lettenmaier DP (2003) Adjustment of global gridded precipitation for systematic bias. J Geophys Res 108:4257. doi: 10.1029/2002JD002499

Brown RD, Mote PW (2009) The response of Northern Hemisphere snow cover to a changing climate. J Climate 22:2124–2145

Callaghan TV, Björn LO, Chapin FS III, Chernov Y, Christensen TR, Huntley B, Ims R, Johansson M, Riedlinger DJ, Jonasson S, Matveyeva N, Oechel W, Panikov N, Shaver G (2005) Arctic tundra and polar desert ecosystems. In: Symon C et al. (eds) Arctic climate impact assessment. Cambridge University Press, Cambridge, pp 243–352

Choi G, Robinson DA, Kang S (2010) Changing Northern Hemisphere snow seasons. J Climate 23:5305–5310

Christensen JH, Christensen OB (2007) A summary of the PRUDENCE model projections of changes in European climate by the end of this century. Clim Change 81(Supplement 1):7–30

Collins M, Booth BB, Bhaskaran B, Harris GR, Murphy JM, Sexton DMH, Webb MJ (2010) Climate model errors, feedbacks and forcings: a comparison of perturbed physics and multi-model ensembles. Clim Dyn. doi:10.1007/s00382-010-0808-0

Déqué M, Rowell DP, Lüthi D, Giorgi F, Christensen JH, Rockel B, Jacob D, Kjellström E, de Castro M, van den Hurk B (2007) An intercomparison of regional climate simulations for Europe: assessing uncertainties in model projections. Clim Change 81(Supplement 1):53–70

Elsasser H, Bürki R (2002) Climate change as a threat to tourism in the Alps. Clim Res 20:253–257

Hurrell J (1995) Decadal trends in the North Atlantic Oscillation: regional temperatures and precipitation. Science 269:676–679

Jylhä K, Fronzek S, Tuomenvirta H, Carter TR, Ruosteenoja K (2008) Changes in frost, snow and Baltic Sea ice by the end of the twenty-first century based on climate model projections for Europe. Clim Change 86:441–462

Lemke P, Ren J, Alley R, Allison I, Carrasco J, Flato G, Fujii Y, Kaser G, Mote P, Thomas R, Zhang T (2007) Observations: changes in snow, ice and frozen ground. In: Solomon S et al (eds) Climate Change 2007: the physical science basis. Cambridge University Press, Cambridge, pp 337–383

Makkonen L, Ruokolainen L, Räisänen J, Tikanmäki M (2007) Regional climate model estimates for changes in Nordic extreme events. Geophysica 43:25–48

Meehl GA, Stocker TF, Collins W, Friedlingstein P, Gaye A, Gregory J, Kitoh A, Knutti R, Murphy J, Noda A, Raper S, Watterson I, Weaver A, Zhao Z-C (2007) Global climate projections. In: Solomon S et al (eds) Climate change 2007: the physical science basis. Cambridge University Press, Cambridge, pp 747–845

Mitchell TD, Jones PD (2005) An improved method of constructing a database of monthly climate observations and associated high-resolution grids. Int J Climatol 25:693–712

Mote PW (2006) Climate-driven variability in mountain snowpack in western North America. J Climate 19:6209–6220

Mote PW, Hamlet AF, Clark MP, Lettenmaier DP (2005) Declining mountain snowpack in western North America. Bull Amer Meteor Soc 86:39–49

Nakićenović N, Swart R (eds) (2000) Emission scenarios. A special report of working group III of the Intergovernmental Panel on Climate Change. Cambridge University Press

Räisänen J (2001) CO_2-induced climate change in CMIP2 experiments: quantification of agreement and role of internal variability. J Climate 14:2088–2104

Räisänen J (2008) Warmer climate: less or more snow? Clim Dyn 30:307–319

Räisänen J, Hansson U, Ullerstig A, Döscher R, Graham LP, Jones C, Meier M, Samuelsson P, Willén U (2003) GCM driven simulations of recent and future climate with the Rossby Centre coupled atmosphere—Baltic Sea regional climate model RCAO. Reports Meteorology and Climatology 101, SMHI, Norrköping, Sweden

Räisänen J, Hansson U, Ullerstig A, Döscher R, Graham LP, Jones C, Meier HEM, Samuelsson P, Willén U (2004) European climate in the late 21st century: regional simulations with two driving global models and two forcing scenarios. Clim Dyn 22:13–31

Reuna M (1994) An operational grid method for estimation of the areal water equivalent of snow. Geophysica 30:107–121

Scherrer SC, Appenzeller C, Laternser M (2004) Trends in Swiss alpine snow days—the role of local and large-scale climate variability. Geophys Res Lett 31:L13215. doi:10.1029/2004GL020255

Seager R, Kushnir Y, Nakamura J, Ting M, Naik N (2010) Northern Hemisphere winter snow anomalies: ENSO, NAO and the winter of 2009/10. Geophys Res Lett 37:L14703. doi:10.1029/2010GL043830

Ungersböck M, Rubel F, Fuchs T, Rudolf B (2001) Bias correction of global daily rainge gauge measurements. Phys Chem Earth B26:411–414

van der Linden P, Mitchell JFB (eds) (2009) ENSEMBLES: climate change and its impacts: summary of research and results from the ENSEMBLES project. Met Office Hadley Centre, FitzRoy Road, Exeter EX1 3 PB, UK

Vavrus S (2007) The role of terrestrial snow cover in the climate system. Clim Dyn 29:73–88

Venäläinen A, Kangas M (2003) Estimation of winter road maintenance costs using climate data. Meteorol Appl 10:69–73